Detection and Correction of Blinking Bias in Image Correlation Transport Measurements of Quantum Dot Tagged Macromolecules

Nela Durisic,* Alexia I. Bachir,† David L. Kolin,† Benedict Hebert,* B. Christoffer Lagerholm,‡ Peter Grutter,* and Paul W. Wiseman*†

Departments of *Physics and †Chemistry, McGill University, Montreal, Quebec, Canada; and ‡MEMPHYS, Center for Biomembrane Physics, Department of Physics, University of Southern Denmark, Odense, Denmark

ABSTRACT Semiconductor nanocrystals or quantum dots (QDs) are becoming widely used as fluorescent labels for biological applications. Here we demonstrate that fluorescence fluctuation analysis of their diffusional mobility using temporal image correlation spectroscopy is highly susceptible to systematic errors caused by fluorescence blinking of the nanoparticles. Temporal correlation analysis of fluorescence microscopy image time series of streptavidin-functionalized (CdSe)ZnS QDs freely diffusing in two dimensions shows that the correlation functions are fit well to a commonly used diffusion decay model, but the transport coefficients can have significant systematic errors in the measurements due to blinking. Image correlation measurements of the diffusing QD samples measured at different laser excitation powers and analysis of computer simulated image time series verified that the effect we observe is caused by fluorescence intermittency. We show that reciprocal space image correlation analysis can be used for mobility measurements in the presence of blinking emission because it separates the contributions of fluctuations due to photophysics from those due to transport. We also demonstrate application of the image correlation methods for measurement of the diffusion coefficient of glycosyl phosphatidylinositol-anchored proteins tagged with QDs as imaged on living fibroblasts.

INTRODUCTION

Fluorescence microscopy is the most commonly used method for imaging studies of dynamic processes in living cells; moreover, fluorescence-based biophysical methods are also widely employed. Consequently, there has been much research devoted to developing novel fluorescent probes for these types of applications. Advances in nanoscience have led to the development of photostable luminescent semiconductor nanocrystals or quantum dots (QDs) that have been touted as superior probes for biological imaging applications (1–3). The QDs typically consist of an inorganic semiconductor core and shell (e.g., CdSe/ZnS) with an outer organic coating for water solubility and biocompatibility. Recent improvements in QD synthesis and surface functionalization strategies have made the conjugation of QDs to various biomolecules more feasible, thus increasing their applications to cell and animal biology (4–8). Some of the photophysical properties of QDs are superior to conventional organic fluorophores. In particular, their broad absorption spectra and high quantum yields make them significantly brighter than many common fluorescent dyes (9), while their greater photostability permits longer observation times than conventional organic fluorophores (10,11). Additionally, experiments have shown that QDs have very large two-photon absorption cross sections, which make them promising labels for multiphoton microscopy applications (12).

These photophysical properties of luminescent nanoparticles would also be advantageous for optimizing fluorescence fluctuation measurements of macromolecular transport coefficients using techniques such as fluorescence correlation spectroscopy (FCS) and its imaging analog temporal image correlation spectroscopy (TICS) (13–16). In fluorescence fluctuation methods, the signal/noise ratio increases as the number of fluorescence photons emitted per molecule per second increases (17,18), so having a label with a large quantum yield and absorption cross section is desirable. The enhanced photostability of the QDs is also advantageous for fluorescence fluctuation measurements because photobleaching of the fluorophore can lead to systematic errors in transport coefficients measured by temporal correlation analysis (19).

However, the photophysics of QDs is also characterized by nonstationary emission or fluorescence intermittency that is commonly referred to as luminescent ''blinking'' (20). As techniques such as FCS and TICS measure molecular transport parameters by temporal correlation analysis of fluorescence fluctuations, it is not surprising that the blinking emission of QDs will contribute to the decay of the calculated time correlation function (21,22). The usual goal of an FCS or TICS experiment is to measure the transport coefficients of a labeled macromolecule by correlation analysis of the detected fluorescence fluctuations arising from changes in the number of fluorophores in a laser beam focus as the macromolecules move in and out of the focal region (see Fig. 1, *A* and *B*). However, the luminescent blinking of the QDs will contribute additional fluctuations to the intensity time record (Fig. 1 *B*).

In principle, it is possible to model the decay of time correlation function by including kinetic terms that incorporate the contributions of all microscopic processes that

Submitted February 20, 2007, and accepted for publication April 16, 2007.

Address reprint requests to Nela Durisic, E-mail: nduris@po-box.mcgill.ca.

Editor: Enrico Gratton.

0006-3495/07/08/1338/09 $2.00

doi: 10.1529/biophysj.107.106864

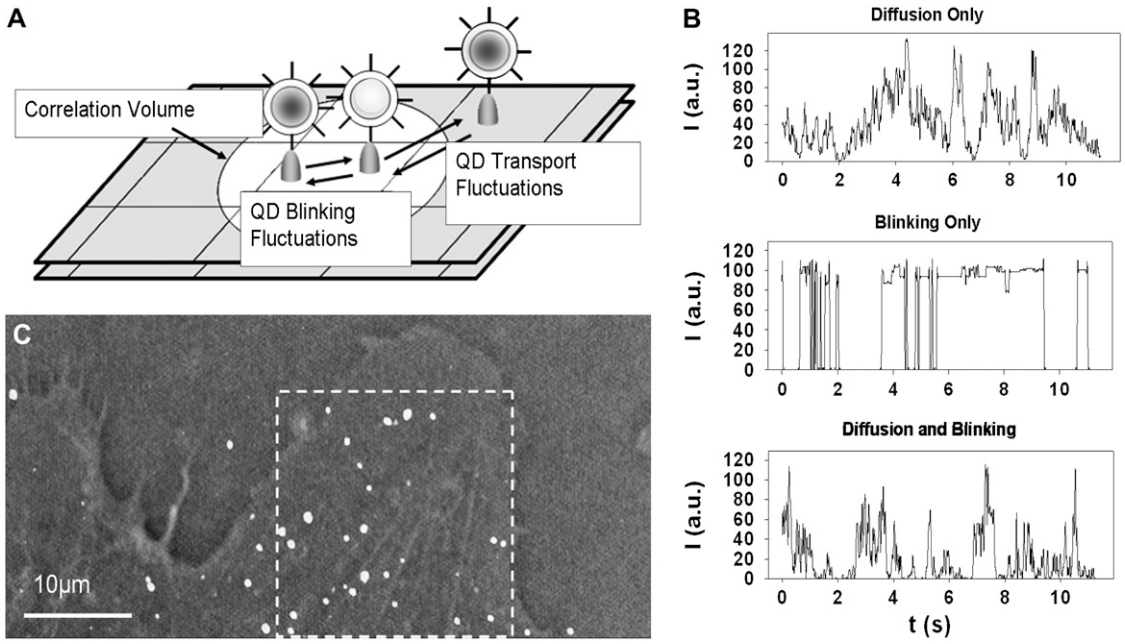

FIGURE 1 (*A*) Schematic representation of the correlation volume on an area detector. Fluorescent fluctuations due to QD mobility cannot be distinguished from blinking since they both result in a change in the signal level from the correlation volume. (*B*) Intensity time traces of a single pixel from three different simulations: in the first simulation, fluorescent particles were diffusing in two dimensions but blinking was absent; in the second, particles with power law blinking were immobilized; and in the third simulation, fluorescent particles were diffusing and blinking. All simulations contained 500 images, each with an image area of 128 × 128 pixels and temporal sampling of 10 frames/s. The diffusion coefficient was set to 0.1 $\mu m^2/s$ and the PDF blinking exponent was $m_{on} = 1.5$. (*C*) Superimposed differential interference contrast and fluorescence image of CD73 protein labeled with QDs in the basal membrane of a fibroblast. The subregion analyzed is outlined in white. It contained 1798 images collected at the video rate.

contribute fluorescence fluctuations on the timescale of the sampling (23). However, unlike many organic dyes (24) and fluorescent proteins (25) (where similar blinking fluctuations have exponential kinetics with time constants usually one order of magnitude smaller than the characteristic molecular diffusion time), QD blinking is especially difficult to separate from other fluctuations of interest since the probability distribution function (PDF) of the ''on'' and ''off'' blinking time durations has a form of inverse power law (26,27):

$$P(t_{On/Off}) \propto \frac{1}{t_{On/Off}^{m_{On/Off}}}. \quad (1)$$

This power law distribution entails that fluctuations due to blinking will occur over many timescales, and this prevents any characteristic correlation time from being linked with the blinking emission via correlation analysis. We thus predict that QD blinking will contribute a systematic error to mobility measurements made by TICS depending on the actual PDF of the nanoparticle blinking.

In our previous work, we showed that the blinking of static QDs immobilized on glass substrates could be studied by TICS to characterize the decay rates of blinking autocorrelation (22). In this work, we show that fluctuations due to luminescent blinking of the QDs will systematically bias transport measurements made by TICS when such nanoparticles are employed as labels. Using a model system of QDs diffusing between two coverslips in a glycerol medium, we were able to obtain total internal reflection fluorescence (TIRF) microscopy image time series with different laser excitation powers to systematically adjust the exponent of the blinking power law (20,28). Analysis of these image series by TICS illustrated that the change in blinking clearly affected the correlation function decay; moreover, a simple two-dimensional (2D) diffusion model fit the decays well but yielded different characteristic diffusion times for the different excitation powers. The experimental results were corroborated by computer simulations of image series of blinking/diffusing point emitters where the blinking, transport, and collection conditions were systematically controlled. The experimental and simulation image series were also analyzed using the new k-space image correlation spectroscopy (kICS), which separates the contributions of fluctuations due to photophysics from those due to transport (29). We show that the transport coefficients can be accurately recovered by kICS without the systematic and hidden bias of the photophysical fluctuations that perturb the temporal image correlation. Finally we demonstrate the application of TICS and kICS to measure the diffusion of a glycosyl phosphatidylinositol (GPI)-anchored protein, CD73, in the membrane of IMR-90 fibroblasts and compare the results to those obtained for the model system and the simulations.

MATERIALS AND METHODS

Model sample preparation

Streptavidin-functionalized (CdSe)ZnS QDs (QD605-streptavidin, Invitrogen Canada, Burlington, Ontario, Canada) with emission wavelength centered at 605 nm were used in all model system experiments. We prepared sample chambers for the model diffusive transport measurements by etching 100-nm deep wells in 10 mm × 10 mm glass coverslips (Fisher Scientific, Ottawa, Ontario, Canada). Before use, all coverslips were boiled in a 1:1 ethanol and chloroform mixture for 30 min, rinsed with copious amounts of milliQ water (Millipore, Bedford, MA), and treated with 30% bovine serum albumin (BSA) solution (Sigma Aldrich, Oakville, Ontario, Canada) as a blocking step to reduce nonspecific adhesion of the QDs to the glass. Stock QD solution was first diluted by a factor of 10^7 in milliQ water and mixed with glycerol so that the final density was ~150 QDs per 1 μL of glycerol water mixture. The mixture was then sonicated for 30 min before being deposited on the etched wells. A second coverslip was placed on top to close the wells, and the assembly was sealed and mounted on a microscope slide for fluorescence imaging. These samples provided a reasonable model for 2D diffusion because the QDs diffused within the 100-nm wells and were imaged by TIRF with an ~100 nm depth of field.

Total internal reflection fluorescence microscopy imaging

All fluorescence microscopy measurements on the model QD samples were conducted on a home-built total internal reflection microscope described in detail previously (22). The samples were mounted on an inverted microscope (Zeiss Axiovert S100TV, Jena, Germany) equipped with a Zeiss Planapo 63× 1.45 numerical aperture oil immersion objective lens and illuminated by through-objective evanescent mode with the 488-nm line from a CW Ar^+ laser (Melles Griot 35 LAP 431, Ottawa, Ontario, Canada). The excitation power was attenuated using neutral density filters. A Q 495 Lp dichroic mirror and 605/55 nm emission filter combination (Chroma Technology, Rockingham, VT) were used for all measurements. The back collected fluorescence was focused onto an intensified PentaMax charge-coupled device (CCD) camera (Princeton Instruments, Trenton, NJ) with 50–70 ms integration time and 13 ms readout time for imaging. Rectangular subregions chosen for correlation analysis were all selected from within the center of the imaged field of view where the evanescent excitation intensity was fairly (~10%) constant.

Computer simulations

Computer simulated image time series of point emitters were generated using programs written in either IDL (RSI, Denver, CO) or MATLAB R14 (The MathWorks, Natick, MA). The programs placed point emitters at random pixel positions with a set particle density of six emitters/μm^2. The particle matrix was convolved with a 2D Gaussian function of defined radius to yield an image matrix. In all simulations, we set the image size either to 64 × 64 or to 128 × 128 pixels with 0.1-μm pixel diameter, and the radius of the Gaussian convolution function was set to three pixels (i.e., 0.3 μm). An image time series was generated in which the diffusion coefficients and the on/off emission statistics of the point emitters were input by the user. For diffusion simulations, periodic boundary conditions were used at the image boundaries, and displacements in x and y were computed at every time step for each particle, according to normally distributed, floating-point, pseudo-random numbers with a mean of zero and a standard deviation of $\sigma = \sqrt{2D\Delta t}$ where D is the diffusion coefficient and Δt the time step between images. The ''on'' and ''off'' time durations for particle emission were randomly selected according to inverse power law probability distributions with a set off time distribution exponent (m_{off}) of 1.5 and on-time distributions exponents (m_{on}) varying between 1.5 and 2. The minimum ''on'' and ''off'' times were set to the image time step of the simulation and for each set of distribution exponents, we varied the time step between images between 2.25 and 100 ms. The simulation image series were then analyzed by both temporal and k-space image correlation techniques.

Cell tissue culture, labeling, and imaging

IMR-90 human fibroblasts (ATCC) were grown in Dulbecco's modified Eagle's medium (D-MEM; Invitrogen, Carlsbad, CA) supplemented with 10% fetal bovine serum (FBS), 100 units/mL penicillin, 100 μg/mL streptomycin, and 0.1 mM minimum essential amino acids. One to two days before an experiment cells were plated in 35-mm glass bottom culture dishes (MatTek, Ashland, MA).

Cells in glass bottom dishes were washed in phosphate buffered saline (PBS) containing 1 mM $CaCl_2$ and 1 mM $MgCl_2$. Cells were subsequently stained with 1 mL of 9.5 μg/mL monoclonal mouse anti-human CD73 (clone AD2, kind gift of N. L. Thompson, Oklahoma Medical Research Foundation, Oklahoma City, OK) and 0.5 μg/mL of the same biotinylated antibody (3.8 biotin/IgG (immunoglobulin G)) in PBS with 1% BSA for 10 min. Cells were then washed in PBS and stained with 100 μL of 2 nM steptavidin-conjugated 605-nm QDs (sAv605-Qdots; Invitrogen) in PBS with 1% BSA for 1 min after which a few drops of a biotin blocking solution (Streptavidin/Biotin Blocking Kit, Vector Laboratories, Burlingame, CA) was added to prevent further cross-linking. Cells were then washed three times in PBS containing free biotin, as before, and finally in D-MEM/F-12 containing 15 mM HEPES but no phenol red (Invitrogen) additionally supplemented with 10% FBS and free biotin. All of these steps were done at room temperature.

Fluorescence time-lapse movies were acquired on an Olympus IX-81 microscope equipped with a XR/MEGA-10Z ICCD (Stanford Photonics, Palo Alto, CA). We used a 100-W Hg-arc lamp and a 460/50 nm excitation filter for exciting the QDs and a 610/20 nm emission filter (Chroma, Rockingham, VT) for detection. Time-lapse sequences were imaged at 30 frames per second.

Image analysis

Temporal image correlation spectroscopy

For a given image time series, $i(x, y, t)$, we define a temporal intensity fluctuation autocorrelation function:

$$r(0,0,\tau) = \frac{\langle \delta i(x,y,t)\delta i(x,y,t+\tau)\rangle}{\langle i(x,y,t)\rangle_t \langle i(x,y,t+\tau)\rangle_{t+\tau}}, \quad (2)$$

where $\delta i(x,y,t) = i(x, y, t) - \langle i(x, y, t)\rangle_t$ is the fluorescence intensity fluctuation at pixel location (x, y) in the image recorded at time t, τ is the temporal lag variable, and ''$\langle\ \rangle$'' denote spatial averaging over all pixel positions in an image (16).

The temporal autocorrelation decay can be fit by a variety of models depending on the dynamic processes that contribute fluctuations on the timescale of the image sampling. We fit our data to the standard 2D diffusion model (16):

$$r(0,0,\tau) = g(0,0,0)\left(1+\frac{\tau}{\tau_d}\right)^{-1} + g_\infty. \quad (3)$$

The fit parameters are the zero lag amplitude, $g(0,0,0)$, the characteristic diffusion time, τ_d, and an offset, g_∞. The diffusion coefficient, D, is calculated from the characteristic diffusion time and the mean beam radius:

$$D = \frac{\langle \omega_0 \rangle^2}{4\tau_d}. \quad (4)$$

The mean beam radius, $\langle \omega_o \rangle$, is calculated from the beam radii obtained by fitting spatial correlation functions to each image in the series as has been described previously (16).

k-Space image correlation spectroscopy

The details of the kICS method were recently published (29). Briefly, a k-space time correlation function, $r_k(\mathbf{k},\tau)$, is obtained by temporal correlation of the image series after 2D spatial Fourier transforms have been calculated for each image:

$$r_k(\mathbf{k},\tau) = \langle \tilde{i}(\mathbf{k},t)\tilde{i}^*(\mathbf{k},t+\tau)\rangle, \quad (5)$$

where $\tilde{i}(\mathbf{k},t)$ is the Fourier transform of the image acquired at time t, $\tilde{i}^*(\mathbf{k},t)$ denotes its complex conjugate, and the angular brackets denote temporal averaging in this case. For a system undergoing 2D diffusion, $r_k(\mathbf{k},\tau)$ has the following analytical form:

$$r_k(\mathbf{k},\tau) = NI_0^2q^2\langle\Theta(t)\Theta(t+\tau)\rangle \exp\left[-D\tau|\mathbf{k}|^2\right](\Omega(\mathbf{k}))^2, \quad (6)$$

where D is the diffusion coefficient, q is the quantum yield, N is the number of particles in the image, I_0 is the incident laser intensity, and $\Omega(\mathbf{k})$ is the optical transfer function of the imaging system. The fluorescence emission function, $\Theta(t)$ (= 1 for on and = 0 for off), does not depend on spatial coordinates and it models the photophysics of the fluorophore assuming that fluorescence emission is independent of other dynamic processes. By dividing $r_k(\mathbf{k},\tau)$ by $r_k(\mathbf{k},0)$ and log transforming, we obtain a point spread function-independent k-space time correlation function:

$$\ln\left[\frac{r_k(\mathbf{k},\tau)}{r_k(\mathbf{k},0)}\right] = \ln[\langle\Theta(t)\Theta(t+\tau)\rangle] - D\tau|\mathbf{k}|^2. \quad (7)$$

For each image series analyzed, D was calculated as follows. First, $\ln[r_k(\mathbf{k},\tau)/r_k(\mathbf{k},0)]$ was circularly averaged. Next, a linear regression of $\ln[r_k(\mathbf{k},\tau)/r_k(\mathbf{k},0)]$ as a function of $|\mathbf{k}|^2$ was performed for each discrete value of τ, yielding slopes of $D\tau$. Finally, the slope of a linear regression of a plot of these slopes as a function of τ was equal to D. Since the diffusion coefficient is calculated independently of fluorescence emission function, the kICS method yields a transport coefficient that is free of systematic errors caused by blinking or other photophysics contributions.

RESULTS AND DISCUSSION

QD blinking systematically affects TICS transport measurements

We imaged streptavidin-functionalized (CdSe)ZnS QDs freely diffusing in two dimensions in the etched coverslip wells by TIRF microscopy at a variety of laser powers but at constant temperature. Other groups have demonstrated that the exponent of the QD blinking power law PDF can change as a function of excitation power (20,28,30). Using the same type of QDs as employed in this study, we have shown previously that temporal correlation functions measured by TICS from samples of static QDs decay more rapidly as the illumination laser power is increased (22). We found that the decay of the temporal autocorrelation function measured for an ensemble of immobilized blinking QDs was fit well by a power law:

$$r(\tau) = A - B\tau^{\alpha}. \quad (8)$$

The fitting exponent α reflects the variation in the underlying ''on'' time distribution and it can be related to the ''on'' time blinking PDF exponent m_{on} as $\alpha = 2 - m_{on}$ (31,32), and it decreases as excitation laser power increases (22). At higher laser powers the QDs blink more frequently and shorter ''on'' events are observed on average, which leads to the observed increased rate of correlation function decay.

We, therefore, expect that the same excitation intensity-dependent decay due to blinking will be manifest in the temporal decay of correlation functions measured by TICS for the diffusing QDs, similar to what has been shown by Weiss and co-workers for faster timescale FCS measurements on semiconductor nanoparticles (21). As with all fluctuation/correlation methods, the relative contribution is going to depend on the sampling timescale, the characteristic transport time, and the blinking time(s). Fig. 2 shows normalized temporal autocorrelation functions measured by TICS from the same sample of diffusing QDs but at two different laser excitation powers: 4.5 W/cm^2 and 13.5 W/cm^2. The overall shape of the autocorrelation functions does not change significantly, but fits of these decays to the standard 2D diffusion model (Eq. 3) yield two different characteristic diffusion times: $\tau_1 = 7.38 \pm 0.05$ s and $\tau_2 = 5.96 \pm 0.06$ s which correspond to $D = (1.88 \pm 0.02) \times 10^{-2}$ μm^2/s and $(2.15 \pm 0.01) \times 10^{-2}$ μm^2/s, respectively, for the lower and higher powers. The average fluorescence intensity per image remained constant throughout the entire stack of 2000 images, thus eliminating the possibility that the differences in the measured D are due to changes in the brightness or bleaching of QDs with time (see *inset* Fig. 2). Transient heating effects caused by 488 nm excitation laser

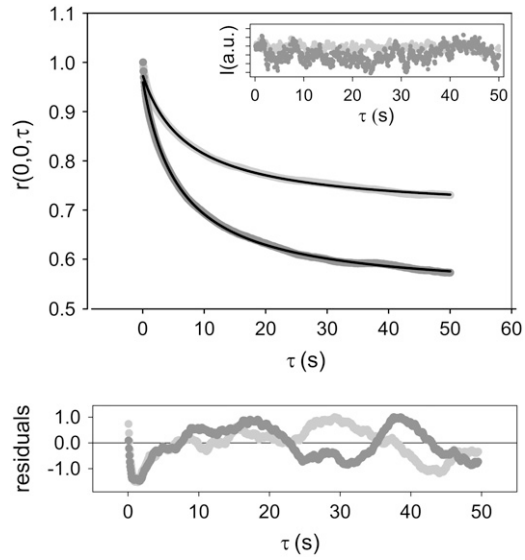

FIGURE 2 Typical normalized intensity time correlation functions for two different excitation powers calculated from the same sample of QDs diffusing and blinking. Excitation laser powers are 4.5 W/cm^2 (*light shaded*) and 13.5 W/cm^2 (*shaded*). Correlation functions and the average fluorescent intensity per frame in the image stack (*inset*) are normalized to 1 for comparison. A fit to 2D-diffusion model is shown in black with residuals for both fits below the plot. Average fluorescence intensity per frame changes from 0.92 to 1.04 and does not decay in time. Each image stack contained 2000 images with 63 ms time resolution.

light were examined earlier for immobilized QDs of similar size (26). As conclusions reached in that study suggest negligible temperature changes due to QD absorption, we expect the diffusion coefficient to be the same for both samples. Clearly, the fluorescence intermittency introduces a systematic error into the TICS measurement obtained with the standard 2D diffusion fit model. More importantly, under these measurement conditions, the temporal autocorrelation functions fit reasonably well to the simple 2D model (see residuals in Fig. 2 *B*) so an experimenter might erroneously assume that blinking was not significant and remain unaware of this systematic deviation due to blinking.

Accurate measurement of diffusion coefficients using image correlation methods

The QD sample that was imaged and analyzed to generate the temporal autocorrelation functions shown in Fig. 2 contained a mixed population of mobile and static nanoparticles. The presence of a static population of fluorescent emitters is known to account for the incomplete decay (offset) of the temporal autocorrelation function as measured by TICS (14). It might be argued that the difference between the TICS measured D at the two different laser powers is really reflecting contributions of the blinking of the static QD population to the decay of the temporal autocorrelation function as we have previously measured this effect for stationary nanoparticles (22). To test whether or not this is the case, we imaged two different model systems of QDs while systematically increasing the excitation laser power. One sample was prepared so that the QDs diffused relatively slowly and were intermixed with a significant fraction (~40%) of immobile nanoparticles. The second sample was prepared so that the QDs were diffusing more quickly (approximately an order of magnitude faster) with almost no static nanoparticles present. Furthermore we analyzed all sets of measurements for both samples by TICS and the reciprocal space variant kICS. It has been previously shown that the transport coefficients measured by kICS are independent of fluorophore photophysics (29). We did not calculate a Stokes-Einstein diffusion coefficient for these samples because it is known that glycerol readily absorbs water, making it difficult to know the true viscosity of the sample, and because our sample chamber geometry was effectively a thin film of ~0.1 μm thickness.

Fig. 3 shows the D as measured by TICS and kICS for the slow/static QD sample as a function of excitation laser power. At the lowest excitation power of 3 W/cm^2 where the contribution of blinking fluctuations should be minimized, there is a systematic difference between the measured $D_{\mathrm{TICS}} = (1.6 \pm 0.2) \times 10^{-2}$ μm^2/s, the TICS measured diffusion coefficient at the same power, and the average diffusion coefficient calculated from the kICS measurements at each power sampled ($\langle D_{\mathrm{kICS}} \rangle = (0.8 \pm 0.2) \times 10^{-2}$ μm^2/s). This difference, where the D_{TICS} is systematically at least 50% greater than $\langle D_{\mathrm{kICS}} \rangle$, is constant for low to moderate laser powers and then begins to increase for powers >31 W/cm^2. This trend shows the interplay between the characteristic transport fluctuation time and the timescales of the nanoparticle blinking which change as a function of laser power. More importantly, it demonstrates that even at the lowest excitation power, there is a systematic error in the TICS measured D for this sample because the measurement did not account for the blinking.

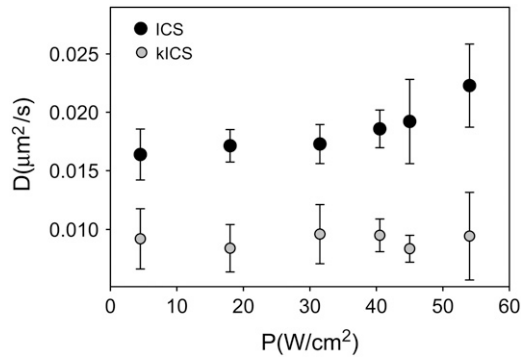

FIGURE 3 Plot of the diffusion coefficient as a function of laser power obtained from the sample that contained a static population of QDs. Diffusion coefficients calculated from TICS analysis (*solid circles*) and from kICS (*shaded circles*). The 2D diffusion model (Eq. 3) is used to fit TICS correlation functions. Each point is an average of six measurements. Error bars are the standard deviation.

The results for the sample containing more rapidly diffusing QDs with a negligible static population are shown in Fig. 4. Again, the TICS measured D increases as a function of laser excitation power, whereas the kICS measured D remains essentially constant within error over the range of powers used for imaging. The average diffusion coefficient calculated from the kICS measurements at each power sampled was $\langle D_{\mathrm{kICS}} \rangle = (8.6 \pm 0.2) \times 10^{-2}$ μm^2/s, and this

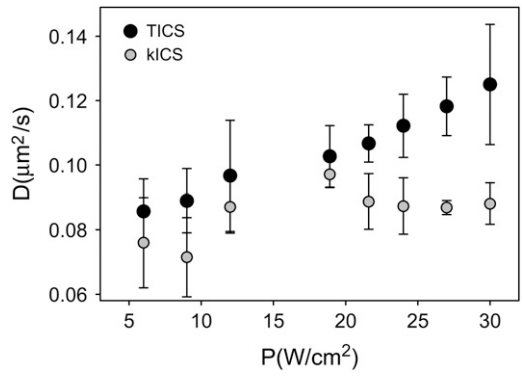

FIGURE 4 Plot of the diffusion coefficient as a function of laser power obtained from TICS analysis for a sample that did not contain a static population of QDs (*solid circles*) when a simple 2D diffusion model is used to fit correlation functions. Diffusion coefficients calculated using kICS analysis are not affected by blinking (*shaded circles*). Each value is an average of four measurements performed on the same sample. Error bars are standard deviations.

value differed from the TICS measured D by almost 50% for the highest powers used. At the lowest laser power, the D_{TICS} is slightly greater than D_{kICS}, but the error bars for these points overlap so the difference is within the statistical uncertainty. This overlap in D_{TICS} and D_{kICS} was not observed at the lowest laser power for the slow/static sample. For both of these samples, we assume that the exponent of the blinking power law distribution will be the same (identical excitation powers), and hence the timescales of the QD emission intermittency will be similar. However, for the slow/static QD sample, the characteristic diffusion time is approximately an order of magnitude larger than that of the rapid/mobile sample. Consequently the blinking fluctuations make a greater contribution to the decay of the TICS autocorrelation function for the slow/static sample because more on/off events can occur during the longer residency time of the QDs within each correlation area. In the rapid/mobile sample, the shorter characteristic diffusion time entails that fewer on/off blinking events are sampled before the QDs exit each correlation area by diffusive transport. Hence the blinking contributes less to the decay of the TICS autocorrelation function and the D_{TICS} and D_{kICS} are the same within the statistical uncertainty. As the laser excitation power is increased, the QD blinking becomes more rapid and the nanoparticles exhibit on/off blinking events of shorter duration so more blinking fluctuations are sampled over the timescale of the characteristic transport time. Hence, we observe that D_{TICS} is systematically greater than D_{kICS} for the higher laser powers for this sample.

The lowest excitation power we used to image the model samples (3 W/cm^2) is similar to the lowest powers used in single-molecule experiments (33). One might be tempted to use higher laser powers to increase the signal/noise ratio in such imaging studies because the QDs are more resistant to photobleaching. However, this would result in a greater systematic error for a TICS diffusion measurement that would not be detected if the standard diffusion fitting model is used. A kICS measurement would detect changes in the blinking statistics as variations in the intercept of the k-space time correlation function and would measure an unbiased diffusion coefficient from the slope of this function (29).

Computer simulation results

We generated computer simulated image time series of point emitters with user set 2D diffusion and on/off emission probability distribution parameters for direct comparison with the model system experimental results and to investigate the role of temporal sampling in more detail. As was observed for the TICS experiments on the model QD samples, the normalized intensity fluctuation time autocorrelation functions calculated from the simulated image time series were well fit by the 2D diffusion model (data not shown), and the characteristic diffusion time decreased as m_{on} increased. Fig. 5 presents the simulation results for the measurement of D_{TICS} and D_{kICS} as a function of m_{on}. As m_{on} increases, the systematic overestimation of the diffusion coefficient measured by TICS increases, whereas the kICS measured transport coefficient matches the set D within statistical error. This trend is completely in accord with our experimental measurements.

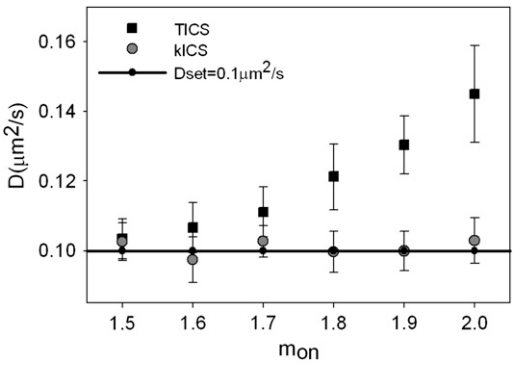

FIGURE 5 Diffusion coefficients calculated from TICS analysis of combined blinking and diffusion simulations of point emitters with varying ''on'' time PDF exponents and an ''off'' time PDF exponent set to 1.5 (*solid squares*). kICS results do not change with ''on'' time PDF exponent (*shaded circles*). Parameters in simulations were set to mimic experimental conditions in model systems that did not contain a static population of QDs. Each image time series was 2000-frames long, with an area of 64 × 64 pixels, time lag of 60 ms between images, and ~250 QDs per frame. The diffusion coefficient was set to 10×10^{-2} μm^2/s. Each value is an average from 20 simulations. Error bars are standard deviations.

The effect of temporal sampling

Previous work has shown that the number of image frames sampled per correlation time (i.e., the ratio of the characteristic transport time, τ_{d}, to the image acquisition time) can determine the precision with which the characteristic correlation time can be measured by TICS (19). It was found that precision was optimized with sampling of two image frames per characteristic time and higher sampling rates did not increase the precision. However, since the QDs have no characteristic blinking timescale, we decided to use the computer simulations to generate image series with a variety of image frame sampling times to determine how this parameter would affect TICS measurements with this type of label. In practice, the frame-to-frame image sampling time can be adjusted over several orders of magnitude in imaging systems equipped with area detectors, by changing the CCD integration time. We adjusted the number of images sampled per characteristic diffusion time from 2.25 to 100 while keeping the total number of images in the time series constant. Fig. 6 shows the TICS measured D as a function of the number of image frames sampled per characteristic diffusion time for two sets of simulations with m_{on} set at 1.5 and 1.8 whereas D was fixed at 0.10 μm^2/s. The results show that the TICS measurement can recover this D within error for a

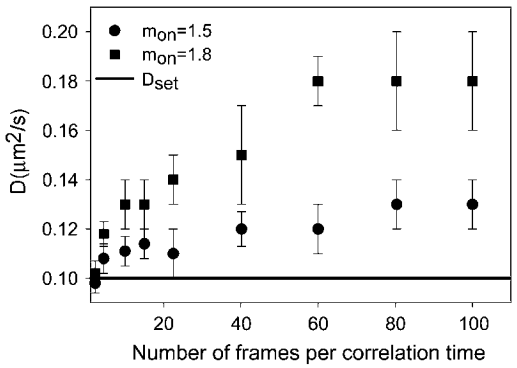

FIGURE 6 Plot of the recovered diffusion coefficient from simulated blinking and diffusing point emitters as a function of the number of frames per characteristic diffusion time when the 2D diffusion model is used to fit TICS data. The diffusion coefficient was set to 0.1 $\mu m^2/s$. ''On'' time PDF exponents are set to 1.5 (*circles*) and 1.8 (*squares*). Error bars are standard deviation calculated from 20 simulations. The image series simulations contained 500 images, each with an image area of 128 × 128 pixels and ~900 particles per frame.

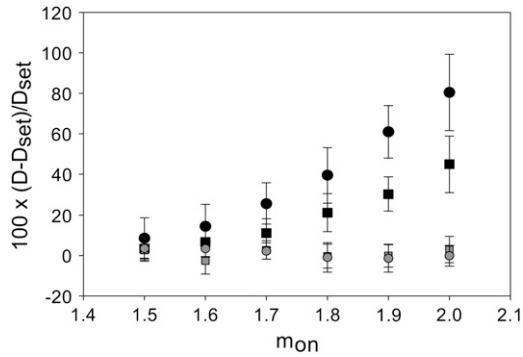

FIGURE 7 Plot of the relative error for recovered diffusion constants from TICS analysis of simulated point emitters blinking and diffusing in two dimensions as a function of ''on'' time PDF exponent for temporal sampling of 13 frames/τ_d (*solid circles*) and 130 frames/τ_d (*solid circles*). kICS results (*solid squares* and *circles*) are insensitive to the blinking regime and temporal sampling. In all simulations $D_{set} = 0.1\ \mu m^2/s$. Error bars are mean ± SD from 20 simulations. The simulations contained 2000 images, each with an image area of 64 × 64 pixels and 250 particles.

temporal sampling ratio of ~2. However, as the sampling ratio is increased, the measured D deviates as an increasing systematic overestimation from the set value. This is due to the fact that it is the faster timescale blinking fluctuations which are now being sampled as the temporal sampling ratio is increased and this contributes to a more rapid decay of the autocorrelation function. In experimental applications, it would not be possible to optimize the temporal sampling without a priori knowledge of the characteristic diffusion time.

To further investigate this effect, we generated simulation image series with a fixed D while varying the m_{on} for the blinking power law distribution and set two different interframe times so that sampling occurred at 13 and 130 frames per characteristic diffusion time. The image series were analyzed by both TICS and kICS to measure the diffusion coefficient. Fig. 7 plots the results as the relative percentage error in the measured diffusion coefficient as a function of m_{on}. Once again, it is clear that the TICS measurement can have a large systematic error depending on the relative contribution of the blinking fluctuations and how frequently they are sampled relative to the characteristic diffusion time. In contrast the kICS measurement recovers the set D with low error and is not affected by the temporal sampling ratio or the blinking fluctuations. This assumes that the imaging rate is sufficiently high that a minimum of two images are recorded per characteristic diffusion time to properly sample the transport process.

Live cell measurements

To compare TICS experiments on cells with results obtained from simulations and model systems, we measured diffusion of CD73 protein labeled with QDs. CD73 or ecto-5′-nucleotidase (5′-NT) is a glycosyl phosphatidylinositol-anchored protein. It is involved in T cell activation (34) and lymphocyte adhesion to the endothelia (35), and its activity has been found to be upregulated in a variety of tumor types (36). Along with other GPI-anchored proteins, CD73 is thought to reside in hypothesized lipid raft nanodomains in the cellular plasma membrane. As such it is one of many potential molecular markers in the ongoing search for in vivo lipid rafts.

To date, most quantitative studies of molecular dynamics with QDs as probes have focused on single particle tracking (SPT) techniques (37). One of the great strengths of fluorescence fluctuation techniques such as TICS is their ability to measure the dynamics of fluorescent particles at a relatively high density. In contrast, SPT can only be performed on samples in which the average particle spacing is significantly greater than the frame-to-frame particle displacements. The region of the membrane of the IMR-90 cell where the analysis was performed is outlined in Fig. 1 *C*. To verify that the CD73 protein is diffusing freely in that region, we examined the trajectories of several QDs whose traces could be resolved using SPT and did not find signs of confined diffusion (data not shown).

We made an effort to minimize QD blinking during data collection, so we could expect TICS and kICS methods to give similar results. The temporal autocorrelation function measured by TICS from the analyzed region of the cell is shown in Fig. 8 *A*. We calculated the diffusion coefficient to be $D_{TICS} = (0.109 \pm 0.008)\ \mu m^2/s$ from a fit of the 2D diffusion model to this correlation function. Analysis of the same image substack using kICS gave $D_{kICS} = (0.088 \pm 0.008)\ \mu m^2/s$. Once again, kICS measures a smaller diffusion coefficient, which is expected since the transport coefficient measured by the reciprocal space method is not affected by photophysical fluctuations. Thus, even for a sample where QD blinking did not appear by eye to be significant,

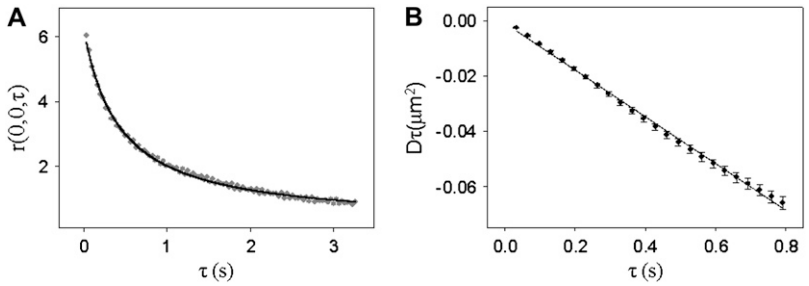

FIGURE 8 (*A*) Experimental temporal autocorrelation function calculated for the 213 × 235 pixels cell region highlighted in Fig. 1 (*shaded circles*). Solid line is a fit to 2D-diffusion model (Eq. 3). Image time series contained 1798 frames with the time step of 33 ms. The precision of the measurement was calculated using Kolin et al. (19). (*B*) Result obtained from kICS analysis. Every point is a slope recovered from Eq. 7 at each time lag τ, $-D\tau$, plotted as a function of τ for a subregion of the cell outlined in white in Fig. 1 *C*. The slope of this plot is $-D_{\mathrm{kICS}}$. The error bars are the error of the corresponding linear regressions.

luminescent blinking of the nanoparticles leads to a small systematic error.

CONCLUSION

We have calculated normalized intensity time correlation function of biocompatible CdSe/ZnS QDs blinking and diffusing in two dimensions and found that it fits well to a decay model that takes only diffusion into account (Eq. 3). However, this approach leads to significant systematic errors in the recovered diffusion coefficients due to QD blinking. We found that the TICS measured diffusion coefficients are highly sensitive to experimental conditions, such as illumination power and temporal sampling, that change the blinking statistics or the sampling of this distribution. We have shown that the kICS measured diffusion coefficients are not affected by QD blinking and that the reciprocal space method is the approach of choice for correlation measurements of transport in 2D systems where nanoparticle densities are high enough to make SPT impractical. We have demonstrated that the kICS approach can also be used to measure the transport of QD labeled receptors on cells with the same advantages as were shown for the model systems.

SUPPLEMENTARY MATERIAL

To view all of the supplemental files associated with this article, visit www.biophysj.org.

P.W.W. and P.G. acknowledge support from the Natural Sciences and Engineering Research Council of Canada (NSERC) and the Canadian Institutes of Health Research (CIHR). P.G. acknowledges Le Fonds Québécois de la Recherche sur la Nature et les Technologies (FQRNT). D.L.K. is grateful for support from a NSERC Canada Graduate Scholarship and N.D. for support from the CIHR Neurophysics training grant program. B.C.L. acknowledges support from Prof. Ken Jacobson and Prof. Nancy Thompson from the University of North Carolina for postdoctoral supervision at the time of the cell experiments and National Institutes of Health grants GM-41402 and GM-64346 and by National Science Foundation grant MCB-0130589.

REFERENCES

1. Bruchez, M. Jr., M. Moronne, P. Gin, S. Weiss, and A. P. Alivisatos. 1998. Semiconductor nanocrystals as fluorescent biological labels. *Science*. 281:2013–2016.
2. Alivisatos, P. 2004. The use of nanocrystals in biological detection. *Nat. Biotechnol.* 22:47–52.
3. Wu, X. Y., J. H. Liu, Q. J. Liu, N. K. Haley, A. J. Treadway, P. J. Larson, F. N. Ge, F. Peale, and P. M. Bruchez. 2002. Immunofluorescent labeling of cancer marker Her2 and other cellular targets with semiconductor quantum dots. *Nat. Biotechnol.* 21:41–46.
4. Pellegrino, T., L. Manna, S. Kudera, T. Liedl, D. Koktysh, L. A. Rogach, S. Keller, J. Rädler, G. Natile, and W. J. Parak. 2004. Hydrophobic nanocrystals coated with an amphiphilic polymer shell: a general route to water soluble nanocrystals. *Nano Lett.* 4:703–707.
5. Gao, X., Y. Cui, M. R. Levenson, K. W. L. Chung, and S. Nie. 2004. In vivo cancer targeting and imaging with semiconductor quantum dots. *Nat. Biotechnol.* 22:969–976.
6. Howarth, M., K. Takao, Y. Hayashi, and A. Y. Ting. 2005. Targeting quantum dots to surface proteins in living cells with biotin ligase. *Proc. Natl. Acad. Sci. USA.* 102:7583–7588.
7. Michalet, X., F. F. Pinaud, L. A. Bentolila, J. M. Tsay, S. Doose, J. J. Li, G. Sundaresan, A. M. Wu, S. S. Gambhir, and S. Weiss. 2005. Quantum dots for live cells, in vivo imaging and diagnostics. *Science*. 307:538–544.
8. Medintz, I. L., H. T. Uyeda, E. R. Goldman, and H. Mattoussi. 2005. Quantum dot bioconjugates for imaging, labelling and sensing. *Nat. Mater.* 4:435–446.
9. Warren, C. W. C., and S. Nie. 1998. Quantum dot bioconjugates for ultrasensitive nonisotopic detection. *Science*. 281:2016–2018.
10. Michalet, X., F. Pinaud, T. D. Lacoste, M. Dahan, M. P. Bruchez, A. P. Alivisatos, and S. Weiss. 2001. Properties of fluorescent semiconductor nanocrystals and their application to biological labeling. *Single Molecules.* 2:261–276.
11. Dubertret, B., P. Skourides, D. J. Norris, V. Noireaux, A. H. Brivanlou, and A. Libchaber. 2002. In vivo imaging of quantum dots encapsulated in phospholipid micelles. *Science*. 298:1759–1762.
12. Larson, D. R., W. R. Zipfel, R. M. Williams, S. W. Clark, M. P. Bruchez, F. W. Wise, and W. W. Webb. 2003. Water-soluble quantum dots for multiphoton fluorescence imaging in vivo. *Science*. 300:1434–1436.
13. Magde, D., E. Elson, and W. W. Webb. 1972. Thermodynamic fluctuations in a reacting system-measurement by fluorescence correlation spectroscopy. *Phys. Rev. Lett.* 29:705–708.
14. Wiseman, P. W., C. M. Brown, D. J. Webb, B. Hebert, N. L. Johnson, J. A. Squier, M. H. Ellisman, and A. F. Horwitz. 2004. Spatial mapping of integrin interactions and dynamics during cell migration by image correlation microscopy. *J. Cell Sci.* 117:5521–5534.
15. Hebert, B., S. Costantino, and P. W. Wiseman. 2005. Spatiotemporal image correlation spectroscopy (STICS) theory, verification, and application to protein velocity mapping in living CHO cells. *Biophys. J.* 88: 3601–3614.
16. Wiseman, P. W., J. A. Squier, M. H. Ellisman, and K. R. Wilson. 2000. Two-photon image correlation spectroscopy and image cross-correlation spectroscopy. *J. Microsc.* 200:14–25.
17. Saffarian, S., and E. L. Elson. 2003. Statistical analysis of fluorescence correlation spectroscopy: the standard deviation and bias. *Biophys. J.* 84:2030–2042.

18. Koppel, D. E. 1974. Statistical accuracy in fluorescence correlation spectroscopy. *Phys. Rev. A.* 10:1935–1945.

19. Kolin, D. L., S. Costantino, and P. W. Wiseman. 2006. Sampling effects, noise, and photobleaching in temporal image correlation spectroscopy. *Biophys. J.* 90:628–639.

20. Nirmal, M., B. O. Dabbousi, M. G. Bawendi, J. J. Macklin, J. K. Trautman, T. D. Harris, and L. E. Brus. 1996. Fluorescence intermittency in single cadmium selenide nanocrystals. *Nature*. 383:802–804.

21. Doose, S., J. M. Tsay, F. Pinaud, and S. Weiss. 2005. Comparison of photophysical and colloidal properties of biocompatible semiconductor nanocrystals using fluorescence correlation spectroscopy. *Anal. Chem.* 77:2235–2242.

22. Bachir, I. A., N. Durisic, B. Hebert, P. Grütter, and P. W. Wiseman. 2006. Characterization of blinking dynamics in quantum dot ensembles using image correlation spectroscopy. *J. Appl. Phys*. 99:064503–064510.

23. Krichevsky, O., and G. Bonnet. 2002. Fluorescence correlation spectroscopy: the technique and its applications. *Rep. Prog. Phys.* 65: 251–297.

24. Ha, T., T. Enderle, D. S. Chemla, P. R. Selvin, and S. Weiss. 1997. Quantum jumps of single molecules at room temperature. *Chem. Phys. Lett*. 271:1–5.

25. Dickson, R. M., A. B. Cubitt, R. Y. Tsien, and W. E. Moerner. 1997. On/off blinking and switching behaviour of single molecules of green fluorescent protein. *Nature*. 388:355–358.

26. Kuno, M., D. P. Fromm, H. F. Hamann, A. Gallagher, and D. J. Nesbitt. 2001. ''On''/''off'' fluorescence intermittency of single semiconductor quantum dots. *J. Chem. Phys.* 115:1028–1040.

27. Kuno, M., P. D. Fromm, F. H. Hamann, A. Gallagher, and J. D. Nesbitt. 2000. Nonexponential ''blinking'' kinetics of single CdSe quantum dots: a universal power law behavior. *J. Chem. Phys.* 112: 3117–3120.

28. Shimizu, K. T., G. R. Neuhauser, A. C. Leatherdale, A. S. Empedocles, K. W. Woo, and M. G. Bawendi. 2001. Blinking statistics in single semiconductor nanocrystal quantum dots. *Phys. Rev. B*. 63:205316–205321.

29. Kolin, D. L., D. Ronis, and P. W. Wiseman. 2006. k-Space image correlation spectroscopy: a method for accurate transport measurements independent of fluorophore photophysics. *Biophys. J*. 91:3061–3075.

30. Kobitski, A. Y., C. D. Heyes, and U. G. Nienhaus. 2004. Total internal reflection fluorescence microscopy—a powerful tool to study single quantum dots. *Appl. Surf. Sci*. 234:86–92.

31. Margolin, G., and E. Barkai. 2004. Aging correlation functions for blinking nanocrystals, and other on-off stochastic processes. *J. Chem. Phys*. 121:1566–1577.

32. Margolin, G., and E. Barkai. 2005. Nonergodicity of blinking nanocrystals and other Lévy-walk processes. *Phys. Rev. Lett*. 94: 080601–080604.

33. Moerner, E. W., and D. P. Fromm. 2003. Methods of single-molecule fluorescence spectroscopy and microscopy. *Rev. Sci. Instr*. 74:3597–3619.

34. Thompson, L. F., J. M. Ruedi, A. Glass, M. G. Low, and A. H. Lucas. 1989. Antibodies to 5′-nucleotidase (CD73), a glycosyl-phosphatidylinositol-anchored protein, cause human peripheral blood T cells to proliferate. *J. Immunol*. 143:1815–1821.

35. Airas, L., J. Hellman, M. Salmi, P. Bono, T. Puurunen, D. J. Smith, and S. Jalkanen. 1995. CD73 is involved in lymphocyte binding to the endothelium: characterization of lymphocyte-vascular adhesion protein 2 identifies it as CD73. *J. Exp. Med*. 182:1603–1608.

36. Sadej, R., J. Spychala, and A. C. Skladanowski. 2006. Ecto-5′-nucleotidase (eN, CD73) is coexpressed with metastasis promoting antigens in human melanoma cells. *Nucleosides Nucleotides Nucleic Acids*. 25:1119–1123.

37. Dahan, M., S. Levi, C. Luccardini, P. Rostaing, B. Riveau, and A. Triller. 2003. Diffusion dynamics of glycine receptors revealed by single-quantum dot tracking. *Science*. 302:442–445.